Impacts of Bulk Phosphorous Content of Electroless Nickel Layers to Solder Joint Integrity and their Use as Gold- and Aluminum-Wire Bond Surfaces

Sven Lamprecht, Kuldip Johal, Hugh Roberts, Dr. Hans-Jurgen Schreier
Atotech Deutschland GmbH, Berlin, Germany
Atotech USA, Inc, Rock Hill, SC, USA
kjohal@atousa.com; sven.lamprecht@atotech.com; hroberts@atousa.com

ABSTRACT

The influence of co-deposited phosphorus within an electroless nickel layer `(from low- to high-P) on the reliability of the solder joint integrity and aluminum-wire bond performance was investigated. The solder joint evaluation was conducted using solder mask-defined and non-solder mask-defined BGAs as test vehicles and using the ball shear technique to establish the level of any "brittle fracture". The type and structure of the intermetallic compound (IMC) created before and after thermal cycling was examined relative to the co-deposited phosphorus (from mid- to high-P) within an electroless nickel layer to determine if there is any influence on solder joint integrity. It was found that as the nickel thickness decreased and the gold thickness increased the highest impact on solder joint integrity was observed. However in the case of higher P content, even at the lower nickel thickness no signs of any brittle fracture were found

.

Two types of IMC were created on the thermo-cycled product using lead-free (Sn-Ag-Cu) solder balls, which were of different structural and chemical composition. The needle-like IMC structure is $(Ni,Cu)_3Sn_4$ with Ag_3Sn co-dispersed into the bulk solder, while the chunky IMC structure is $(Cu,Ni)_6Sn_5$. The phosphorus enrichment after the immersion gold reaction and soldering showed a 30% lower enrichment at the interface of the electroless Nickel / C-Ni-Sn IMC using a high-phosphorus ENIG system. The mid-range phosphorus electroless nickel layer showed a wide spread of all force/length curves as compared to high-phosphorus layers, which were not negatively influenced by 1000 thermal cycles.

For aluminum-wire bonding, no effect is observed by varying the bulk phosphorus content, neither for "as received" nor after 4 hours at 150°C annealing. Gold-wire bonding showed very good results with high-P electroless Nickel with only one-tenth of the gold thickness of that used for electrolytic nickel/gold. Based on this investigation, the recommendation would be to use high-P ENIG system for superior joint reliability.

INTRODUCTION

Within the electronics industry, components and printed circuit boards (PCB) are increasingly adding more requirements to the functionality of the electronic device. At the same time, the environments in which these electronic devices are used are also continuously changing, which in turn is challenging the reliability of the soldered joints and/or wire bonds.

The impact of the operating environment is particularly important for certain functions, such as keypads or contact switches, where areas of the final metallic coating are exposed. Because these areas are not covered by solder and cannot be encapsulated by other protective coatings, they need to withstand corrosive environments, such as high humidity or pollutant gas.

If corrosion occurs, this will interfere with the electrical behavior due to either the electrical conductivity of corrosion products (creating a short), or damage to the final coating (as a contact surface for key pads or contact switches), thus impacting the functionality of final products, leading to low service life.

Due to the above issue, in recent years there has been a consistent growth in the use of high-phosphorous (>9.5-13% wt% P) electroless nickel/immersion gold (HP-ENIG) as a final finish, especially in the telecommunication industry. HP-ENIG offers superior corrosion resistance compared to a low- or medium- phosphorous ENIG process. This finish is now frequently being used for PBGA, CSP, QFP and COB. More recently, HP-ENIG has gained considerable interest as a low-cost, under-bump metallization for flip-chip bumping application.

The final coating on the PCB is one of the key issues for the reliability of the whole assembly. This deposit should act as a long-time diffusion barrier, protecting underlying copper pads at high operating temperatures. The formed intermetallic compounds (IMC) need to handle mismatches in coefficient of thermal expansion (CTE) without resulting in silicon cracks. In addition, the formed metallurgical system should not show any brittleness caused by this IMC formation.

This paper describes the influence of co-deposited phosphorus within an electroless nickel layer (from low- to high-P) on the reliability of the solder joint integrity and aluminum wire-bond performance. The solder joint evaluation was conducted using solder mask-defined and non-solder masked-defined BGAs as test vehicles and using the ball shear technique to

establish the level of any "brittle fracture". The type and structure of the IMC created before and after thermal cycling was also evaluated against the co-deposited phosphorus (from low- to high-P) within an electroless nickel layer to determine if there is any influence on solder joint integrity.

ENIG SYSTEMS

The key variables for testing solder joint reliability were electroless nickel thickness (3µm vs. 6µm), immersion gold thickness (0.06µm vs. 0.14µm) and phosphorous content in the bulk nickel layer. In this investigation, "medium-P" is considered to be 7-9 wt. pct. phosphorus, while "high-P" is considered to be 9.5-13 wt. pct. phosphorus. However due to the high corrosion resistance of the high P electroless nickel, which impacts the immersion gold deposition, it was not possible to obtain a gold thickness greater than 0.06µm under standard operating parameters.

Solder joint formation of nickel/gold surface finishes takes place through gold dissolution into the solder, forming an IMC between the nickel and tin. It is well known that the formed Ni/Sn IMC influences the solder joint integrity. A uniform and dense IMC is essential for a ductile solder joint.

DESCRIPTION OF EXPERIMENT

BGA substrates were prepared by systematically varying ENIG layer thickness and bulk phosphorus content. The layers were characterized by X-ray fluorescence (XRF) and scanning electron microscope (SEM) in a cross-section.

Solderability was determined with a solder balance (Multicore MUST II Solderability Tester), comparing ENIG systems with different bulk phosphorous content.

The following ball shear tests were performed:

- BGA ball (Sn-Ag-Cu) attachment on "as received" samples, comparing fracture behavior of ENIG systems with different bulk phosphorous content.
- After BGA ball (Sn-Ag-Cu) attachment, the samples were exposed to 1000 thermo-cycles (TC) from -55°C to 125°C with dwell times of 15 minutes at each temperature and 3-second transfer times, comparing fracture behavior of ENIG systems with different bulk phosphorous content.

Solder joint integrity was determined by ball shear testing (Dage PC 2400) using solder mask-defined and non-solder mask-defined pads.

The following wire bond pull strength tests were conducted:

- For aluminum-wire bonding, bond pull strength was compared with results "as received" and after annealing at 150°C for four hours. Wire bond pull strength is compared with ENIG systems having different bulk phosphorous content.
- For gold wire bonding, bond pull strength was compared with electrolytic-plated nickel/gold layers and ENIG with a medium- and high-phosphorous content in the bulk nickel layer.

Wire bond pull strength was determined by pull testing (Dage BT 2400 PC) using a hook to lift the bonded wires.

Scanning Electron Microscope

Determination of the bulk phosphorous (P) content of the ENIG layer was performed by cross-sectioning and SEM, since the energy values of phosphorus (Kβ line at 2.139 keV) and gold (Mα line at 2.123 keV) are very similar. Depending on the type and software employed by the SEM it is possible to differentiate the phosphorus from gold. The phosphorus content is expressed in weight percent (wt %).

XRF

The XRF was used to determine nickel and gold thickness. The X-ray fluorescence intensity is proportional to the number of atoms within the probed volume (fraction of a square millimeter, several µm in depth). From this intensity, using the specific gravity of the layer as a proportional constant, the layer thickness is calculated. When the instrument is properly calibrated, the nickel and gold layer thicknesses can be determined.

Solderability

As a control tool on site at the PCB producer, solderability tests (i.e. wetting balance tests) are typically performed on a frequent basis, using either special coupons, samples plated during production or the PCB itself. This test gives a good indication regarding overall quality of the final finishing plating process.

The Multicore MUST II system performs each test with a fresh solder ball, compared to using a solder pot, thus avoiding any solder contamination. The tested samples, as well as the solder ball, are fluxed before the sample is reflow soldered. Results are given for wetting force and wetting time. Additionally a time/force diagram is plotted. Typical values shown are maximum wetting force (F_{max}), time to F_{max}, time to 2/3 F_{max}, force after 2 sec. (F_1) and force after 5 sec (F_2).

Pass/fail criteria within this paper is the time to 2/3 F_{max} which must be less than one second..

Ball Shear Test

Manufacturers and assemblers of the BGA-laminate typically utilize ball shear tests. Because the individual pads are solder mask-defined (SMD), shown in Figure 1, the chance of a pad pull-out is greater in comparison to a non-solder mask-defined (NSMD) pad, as shown in Figure 2, since SMD pads are typically found on the board side. Higher strength against pad pull-out will force the fracture to occur at the metallic layer, the IMC, the solder or any interface in between.

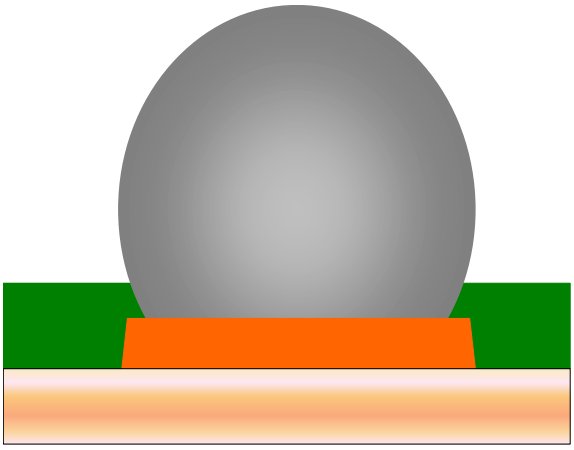

Fig. 1 Solder Mask Defined pad (SMD)

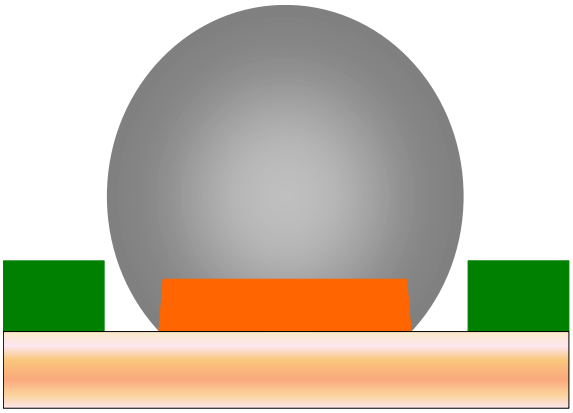

Fig. 2 Non Solder Mask Defined pad (NSMD)

A BGA solder ball (760µm diameter) is soldered onto the SMD pad (600µm diameter opening) or NSMD pad (600µm diameter) and sheared off using a DAGE PC 2400 shear tester. Force/length diagrams are then plotted as presented in Figure 3. Diagrams with a steep descent after the maximum height represent "brittle" interfacial fracture, while a gradual descent represents "ductile" plastic deformation of the solder.

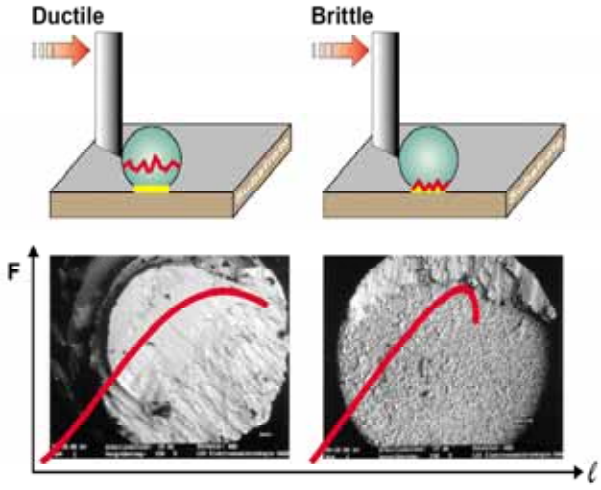

Fig. 3 Schematic diagrams of ball shear test and SEM micrographs of ductile and brittle fracture.

The surface of the remaining pad is analyzed (see Figure 4) and the fracture is classified as "ductile" (fracture in the solder/pad pull-out) or "brittle" (fracture at the IMC). Fracture modes 1 and 4 represent ductile fractures, where the fracture occurs by the shearing of the BGA pad from the PCB (Mode 1) or the fracture occurs within the solder (Mode 4). Brittle fractures occur between the electroless nickel layer and the Ni/Sn IMC (Mode 2) and at the interface between solder and Ni/Sn IMC (Mode 3).

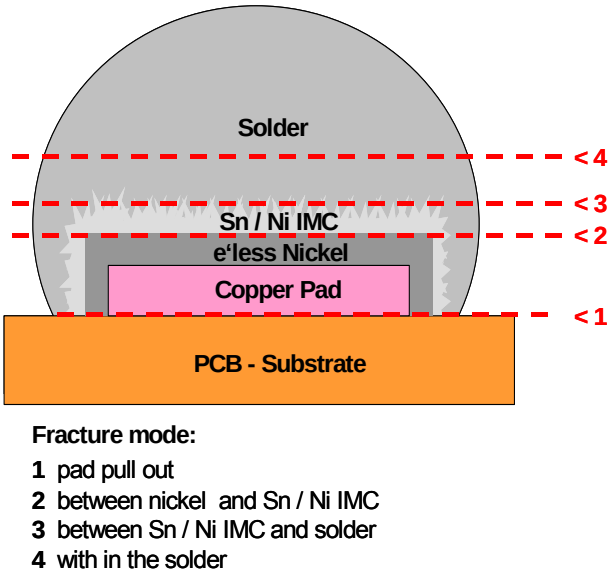

Fig. 4 Classification of fracture modes 1-4 after ball shear test.

In order to clarify the solder joint integrity for the tested ENIG layer systems, samples were prepared as follows:

- Electroless nickel at 3µm to 6µm thickness
  - Medium phosphorous content in the bulk nickel layer at 7-9 wt %
  - High phosphorus content in the bulk nickel layer at 9.5 -13 wt %.
- Immersion gold at 0.05µm to 0.15µm thickness

Samples were assembled with Sn/Pb solder balls (760-µm diameter) using Litton Kester 950 E3.5 (type F-SW33) as flux, in convection reflow oven.
As stated before, high gold thickness was not possible with high P content nickel without operating outside normal conditions.

Wire bond pull strength

Wire bond pull tests were performed using a Dage BT 2400 PC. The maximum pull force, measured in cN, is recorded. Optical inspection of the fracture is then performed to determine the mode of the failure, as shown in Figure 4.
Aluminum wire bonding was performed using 32-µm AlSi-1 wire from Hereaus, while gold wire bonding was performed using 30-µm Au-Beta wire from Hereaus.

TEST RESULTS

Solderability – Multicore MUST II

Figure 5 shows the data for the 156 measurements for each ENIG system. Altering bath age for the respective nickel and gold process solutions, none of the finishes exceeded the fail criteria for time to 2/3 F_{max} of one second.

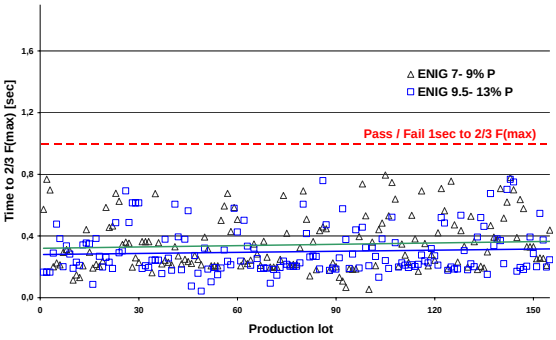

Fig. 5 Diagram for time to 2/3 F_{max} comparing medium- and high-phosphorus ENIG systems.

Ball shear / 600µm SMD pad

Figure 6 shows a series of ball shear results with 600-µm SMD pads. In this example, two ENIG systems are compared, one with a bulk phosphorus content of 7-9%, the other with 9.5-13% P. The plated electroless nickel and immersion gold thicknesses were varied from 3.2µm to 6.1µm and from 0.06µm to 0.15µm, respectively. Solder balls were attached to samples directly after plating.

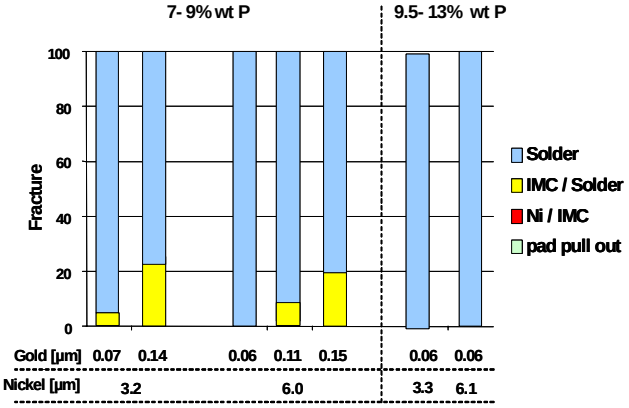

Fig. 6: Detected fracture modes of ENIG layers on 600-µm SMD pads.

Samples with a low gold thickness (0.06µm and 0.07µm) exhibit fracture primarily within the solder (Mode 4). However at low nickel thickness (3.2µm and 3.3µm) in 7-9 % wt P, a low number of Mode 3 fractures occurred, which was not the case for the high-P content nickel.

Samples with low nickel thickness (3.2µm and 3.3µm) and/or samples with high nickel thickness (6.0µm) with high gold thickness (>0.14µm) show the highest number of fractures at the interface between Ni/Sn IMC (Mode 3). In the case of low nickel thickness (3.3µm) with 9.5-13% P, samples exhibited a ductile fracture mode within the solder (Mode 4).

Ball Shear / 600µm NSMD pads

A series of ball shear with 600 µm NSMD pads is shown in Figure 7. As an example, two ENIG systems are compared: one with a bulk P-content of 7-9%, the other with 9.5-13% P. The plated electroless nickel and immersion gold thicknesses varied from 3.2µm to 6.1µm and from 0.06µm to 0.15µm, respectively. Due to the higher corrosion resistance of the high-P, creating a thicker gold layer was not possible without operating the system outside its normal operating parameters. Solder balls were attached to samples directly after plating.

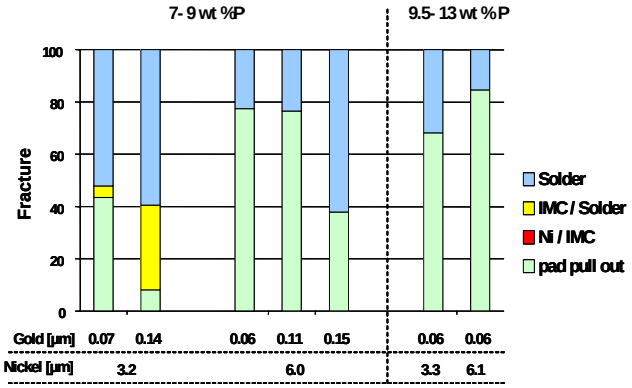

Fig. 7 Detected fracture modes of ENIG layers on 600-µm NSMD pads.

Only samples with P-content of 7-9% in the nickel layer and a nickel thickness of 3.2µm showed brittle fracture (Mode 3) at the interface between the Ni/Sn IMC and the solder, regardless of the gold thickness. Throughout the testing only 600-µm NSMD pads showed fractures of the Mode 1 type with pad pull-out. Nickel layers with 7-9% P, 6.0-µm thickness and 0.15-µm gold thickness exhibited the lowest frequency of pad pull-out, less than 40 percent. By comparison, high-P nickel layers with 6.1-µm thickness and 0.06-µm gold thickness resulted in more than 80 percent pad pull-out.

All samples with an electroless nickel P-content of 9.5-13% (regardless of tested nickel thickness) and 0.06µm gold showed no brittle fractures regardless of the type pad formation (SMD or NSMD). In the case of NSMD pads, even with the thicker immersion gold there were no brittle facture joints. This fact is attributed to the additional anchorage effect of the solder around the pad giving the over joint a greater bond strength.

Solder joint integrity of nickel/gold layers - Phase II.

This part of the investigation involved examining the effect of subjecting a solder ball joint to thermo-cycling by examining the joint integrity and type of IMC that is formed, before and after thermo-cycling. Tests were conducted with 600-µm SMD pads, with lead-free solder balls (Sn-Ag-Cu) and with different

phosphorus contents of 4.2%, 8.0% and 11.2% by weight in the electroless nickel layers.

Ball shear tests on 600-µm pads (before thermo-cycling)

Figures 8, 9 and 10 offer a comparison of force/length diagrams for 600-µm SMD pads at the three different phosphorus contents in the electroless nickel layers.

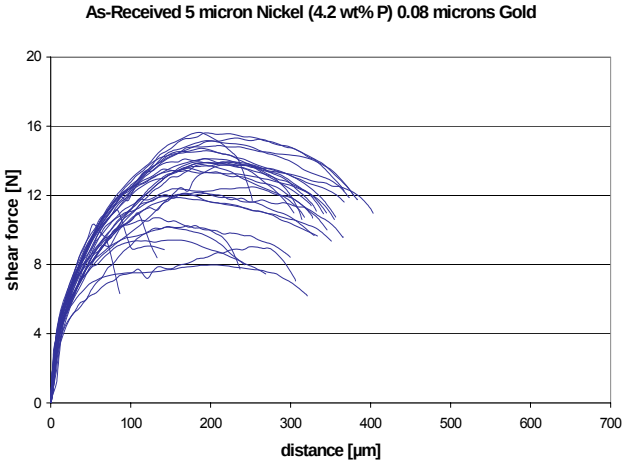

Fig. 8 Ball shear tests on 600-µm pads (before thermo-cycling) 5µm NiP (4.2% P-content), 0.08µm gold

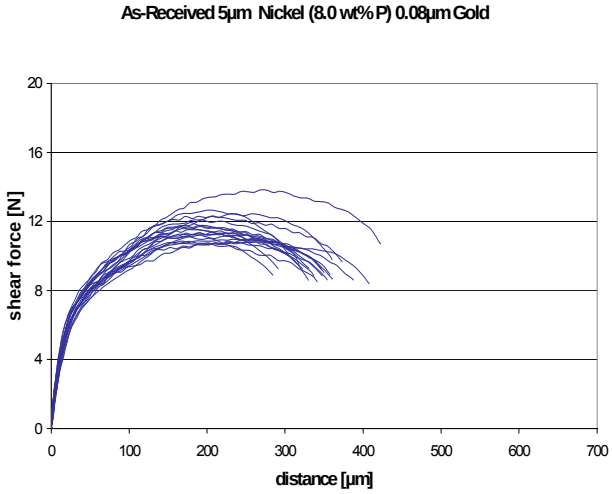

Fig. 9 Ball shear tests on 600-µm pads (before thermo-cycling) 5µm NiP (8.0% P-content), 0.08µm gold

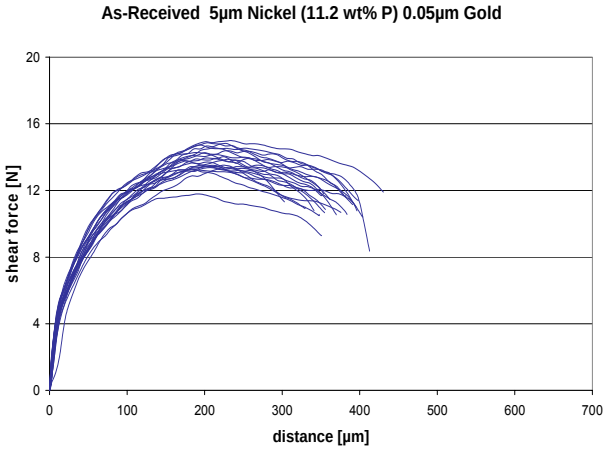

Fig. 10 Ball shear tests on 600-µm pads (before thermo-cycling) 5µm NiP (11.2% P-content), 0.05µm gold

The three nickel systems show a flat descent after the maximum height representing a ductile (i.e. plastic) deformation of the solder. The force/length diagrams for 8.0% P and 11.2% P show a narrow shape of all curves, indicating similar bond characteristics for all tested SMD BGA pads. By comparison, the nickel layer with 4.2% P-content show a wide spread of force/length curves, indicating more variation of total shear force (8N – 16N) for the tested SMD BGA pads.

Ball shear tests on 600-µm pads (after thermo-cycling)

A comparison of force/length diagrams for 600-µm SMD pads at the three different phosphorus contents in the electroless nickel layers is shown in Figures 11, 12 and 13 after thermo-cycling. The lead-free (Sn-Ag-Cu) solder balls were attached to samples directly after plating, followed by 1000 thermo cycles (-55°C / +125°C).

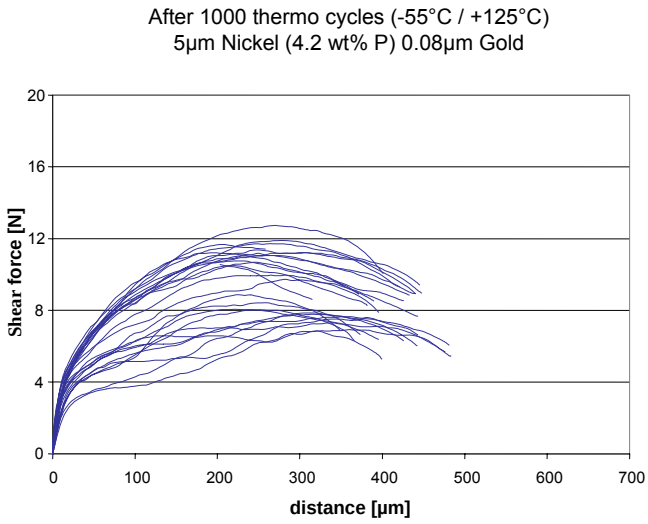

Fig. 11 Ball shear tests on 600-µm pads (after thermo-cycling) 5µm NiP (4.2% P-content), 0.08µm gold

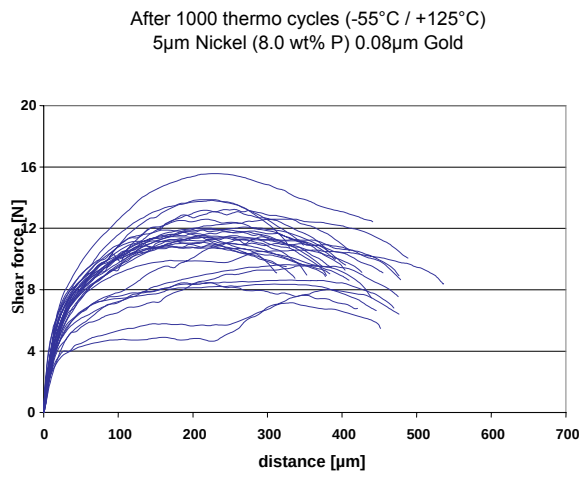

Fig. 12 Ball shear tests on 600-µm pads (after thermo-cycling) 5µm NiP (8.0% P-content), 0.08µm gold

Again, all three nickel systems show a gradual descent after the maximum height, indicative of a ductile deformation of the solder. Only at the 11.2-percent phosphorus content do the force/length diagrams show a narrow shape for all curves.

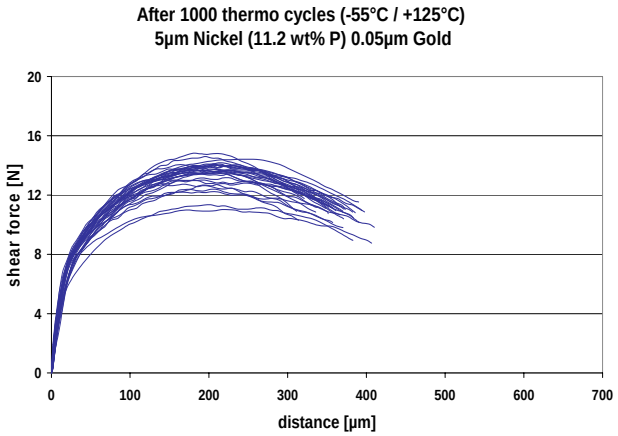

Fig. 13 Ball shear tests on 600-µm pads (after thermo-cycling) 5µm NiP (11.2% P-content), 0.05µm gold

The nickel layers with 4.2% and 8.0% phosphorus show a wide spread of force/length curves, indicating more variation in the total shear force for the tested SMD BGA pads, from 6N to 13N for 4.2% P and from 5N to 16N for 8.0% P.

To evaluate the differences in behavior of the 8.0% P nickel layer compared to the 11.2% P nickel layer, the fractures that occurred were examined by cross-section and EDX. Figure 14 shows the cross-section of the nickel pad with lower phosphorus content, clearly showing fracture within the solder, near the Ni/Sn IMC (Mode 3-4). This example could be classified as a partial brittle fracture.

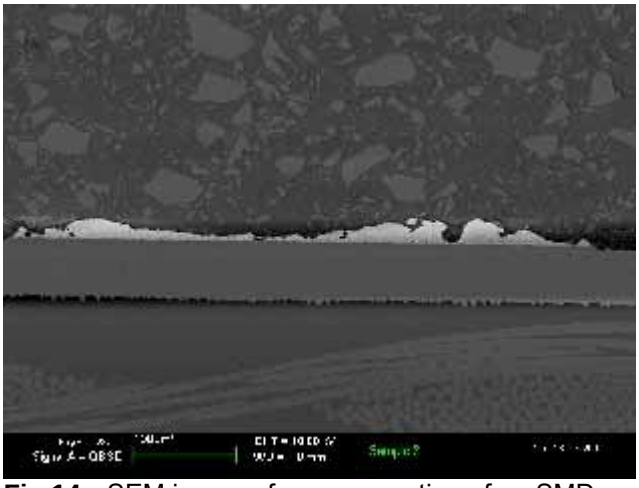

Fig 14 SEM image of a cross-section of an SMD BGA pad after ball shear testing of an 8.0% P nickel layer (Magnification 195x).

By comparison, Figure 15 shows the cross-section of the nickel pad with higher phosphorus content, showing fracture within the solder (Mode 4).

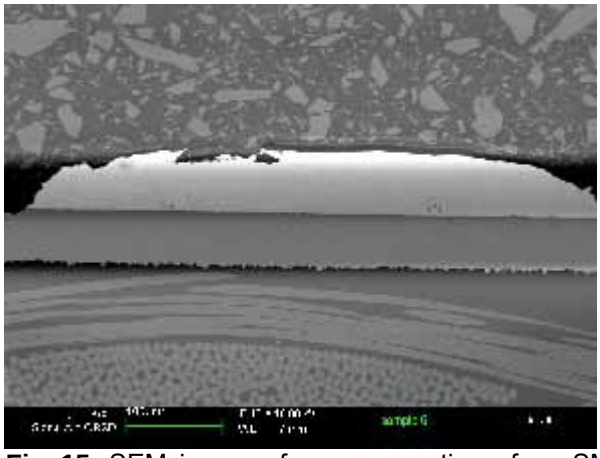

Fig. 15 SEM image of a cross-section of an SMD BGA pad after ball shear testing of an 11.2% P nickel layer (Magnification 195x).

Analysis of IMC before and after thermo cycling

IMCs were formed with a Sn-Ag-Cu alloy using a reflow profile recommended by lead-free solder paste suppliers, as shown in Figure 10. The profile, operating at normal atmosphere, shows a steady temperature increase to 180°C before reaching a peak temperature of 242°C. The total time for the paste in liquid state is 48 seconds.

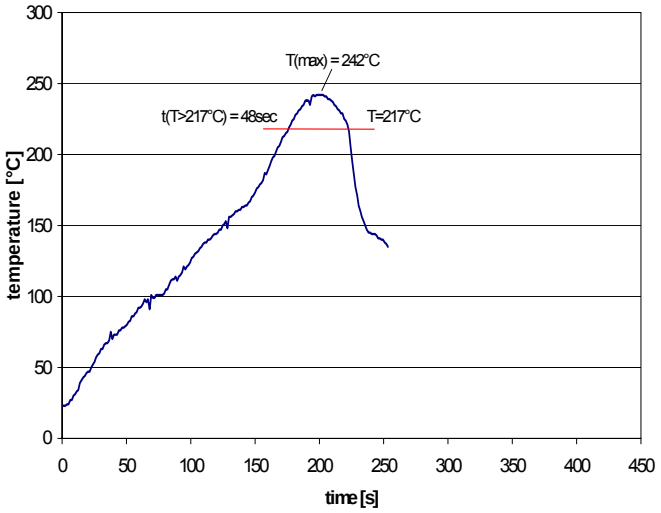

Fig. 16 Reflow profile for Sn-Ag-Cu (lead-free) solder paste

After ball shear testing, the individual solder joint was inspected. To determine the type of intermetallic structure, the sample was stripped of any non-intermetallic solder with a special solution to reveal the IMC structure.

It is evident that the P-content in the bulk electroless nickel is influencing the type of IMC structure that is created during soldering. Comparing the images in Figures 17 and 20 (without thermo-cycling), the IMCs for both the 8.0 % and 11.2 % phosphorus content exhibit a very similar needle-like structure. However, the structure at 8% P-content was larger and less dense than that at 11.2% P.

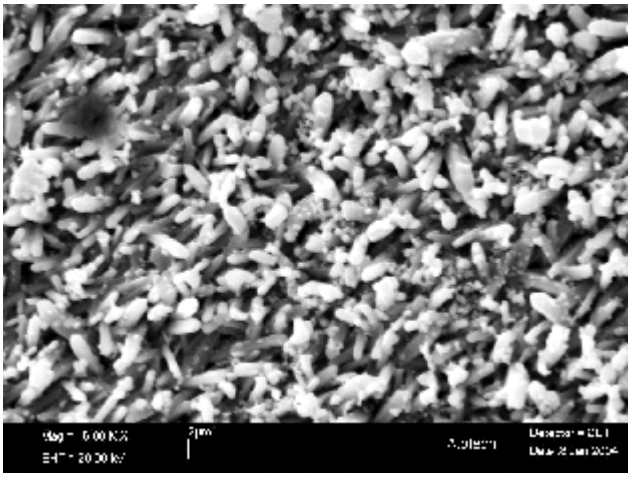

Fig. 17 SEM Image of IMC before thermo-cycling (8.0 wt% P Nickel layer)

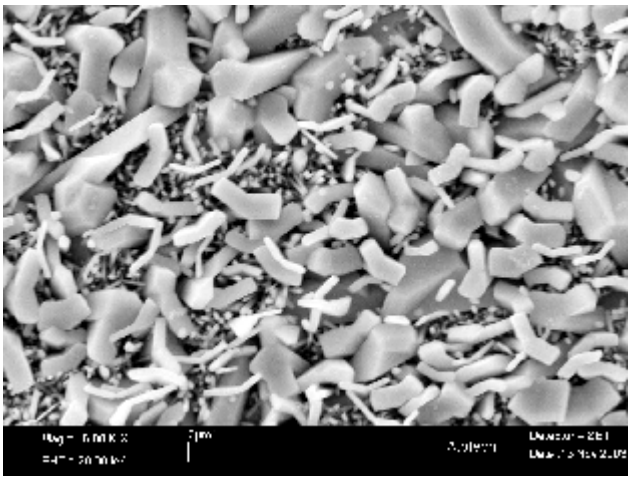

Fig. 18 SEM Image of IMC after 400 thermo-cycles (8.0wt % P Nickel layer)

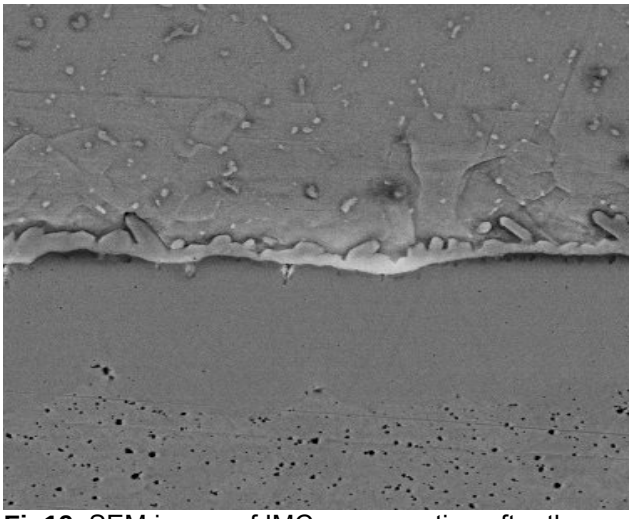

Fig19: SEM image of IMC cross-section after thermo cycling (8.0wt % P Nickel layer)

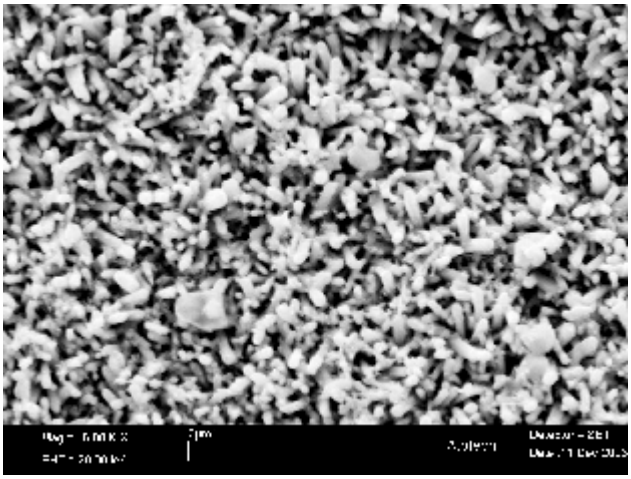

Fig. 20 SEM Image of IMC before thermo-cycling (11.2% P Nickel layer)

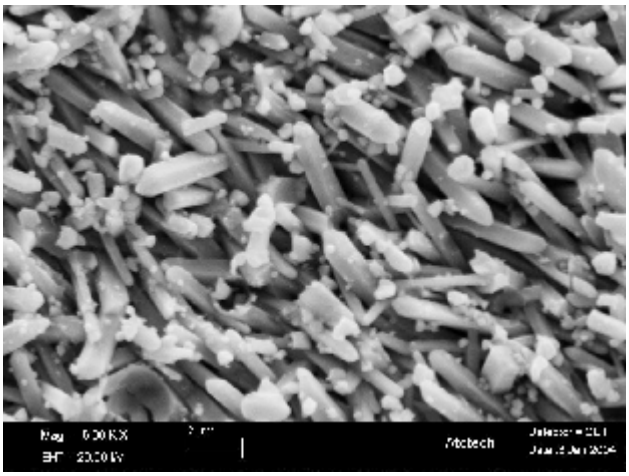

Fig. 21 SEM Image of IMC after 400 thermo cycles (11.2 wt % P Nickel layer)

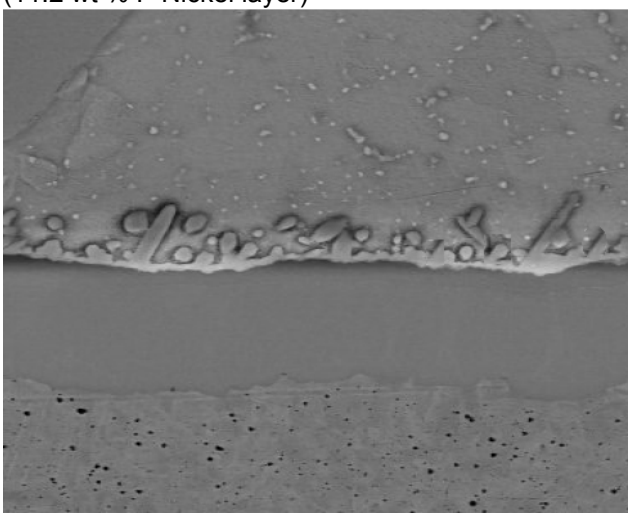

Fig 22: SEM image of IMC cross-section after thermo-cycling (11.2 wt % P Nickel layer)

However, as seen in Figures 18 and 21, after thermo-cycling there is a dramatic change in the IMC structures, particularly in the case for that produced from the 8.0% P-content nickel. The thermo-cycling produces a combination of needle and chunky types of IMC structure. Thermo-cycling of the 11.2% P-content nickel continues to produce a large but denser needle-type of IMC structure. Figures 19 and 22 show the IMC cross-sections after thermo-cycling for the 8.0% P and 11.2% P IMCs.

If the force length/diagrams for the respective ball shear tests are compared, it can be seen that prior to thermo-cycling (Figures 9 and 10) they are very similar in shape, although the 11.2% P-content nickel produces a shear force than is approximately 2-3N higher than the medium P-content nickel. However, after thermo-cycling (Figures 12 and 13), the force/length curves for the 8.0% P show a much wider spread in force ranging from 5 to 16N as compared to the 11.2wt% P, where the force length curves remain fairly constant (11 to 14N).

The next step was to determine the difference in chemical composition between the needle and chunky type of IMC. Considering that lead-free solder balls (Sn-Ag-Cu) were used, following analysis and literature search it was concluded that the needle-like IMC structure is $(Ni,Cu)_3Sn_4$ with Ag_3Sn co-dispersed into the bulk solder. Conversely, the chunky IMC structure is $(Cu,Ni)_6Sn_5$. Figure 23 shows both structures for comparison.

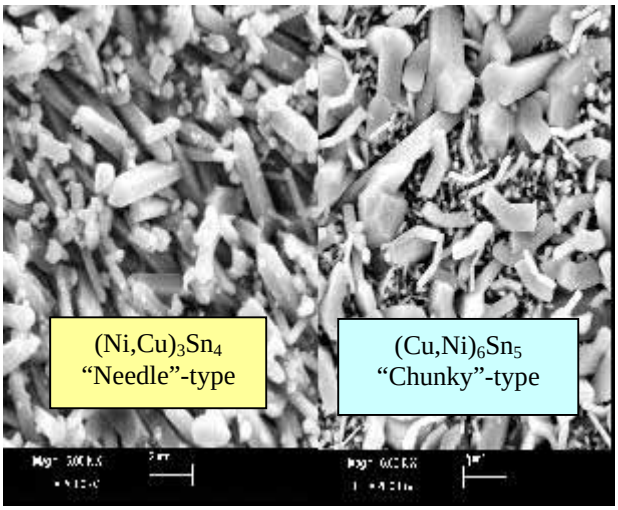

Fig. 23 Different types of IMC produced after 400 thermo-cycles

The chunky-type $(Cu,Ni)_6Sn_5$ IMCs appear to grow at the expense of the needle-type IMCs during thermo-cycling of the solder joint. One possibility is that this growth reflects the influence of Nickel "grain" (growth) boundaries, which are easier to dissolve/attack by the solder. This tendency will be further investigated in an effort to determine the mechanism involved. In addition, use of eutectic solder will also be explored.

Considering that the high P-content (11.2% P) is more corrosion resistant and a slightly lower amount of gold was applied to the electroless nickel surface, a very slight attack from the following gold displacement reaction can be expected.

$$Ni + 2Au^{-} \rightarrow Ni^{2+} + 2Au$$

One could argue that the electroless nickel at 8.0% P-content does have a much rougher (nodule-like) structure and could result in greater attack on the grain boundaries. However, at a gold thickness controlled at 0.08µm, the attack rate on the nickel boundaries would be minimized. Therefore, what must be determined is the phosphorus content before and after soldering to establish which factor influenced the dissolution of the nickel.

SEM images of a plated electroless nickel surface also show a more nodular type of structure for the 8% P nickel (Figure 24) in comparison to the much flatter structure of the nickel with 11.2% phosphorus content (Figure 25).

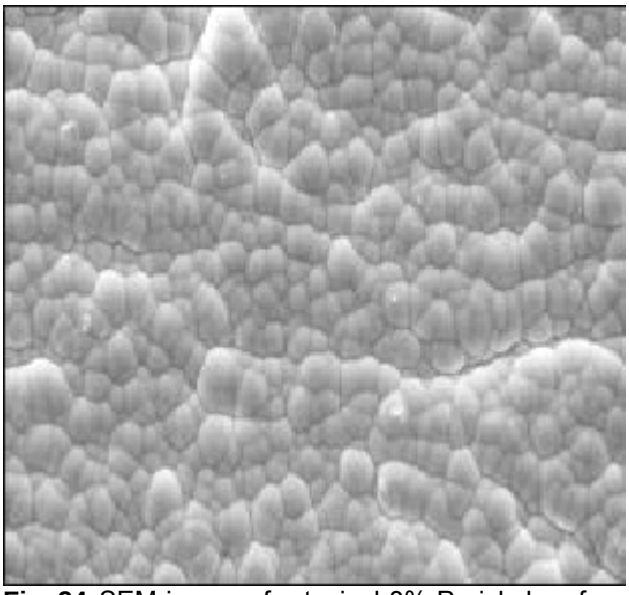

Fig. 24 SEM image of a typical 8%-P nickel surface (Magnification 5000x)

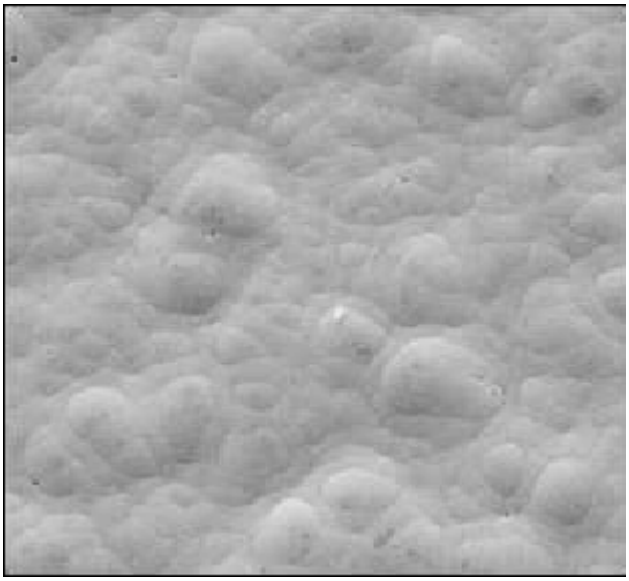

Fig. 25 SEM image of a typical 11.2%-P nickel surface (Magnification 5000x)

P-content enrichment analysis

Figures 26 and 27, respectively, present an analysis of an IMC for an 8% P and 11.2% P nickel layer using a Sn-Ag-Cu solder alloy. The line on the SEM images indicates the area for line scan. On the right side, the quantitative P-content is shown, for the investigated area.

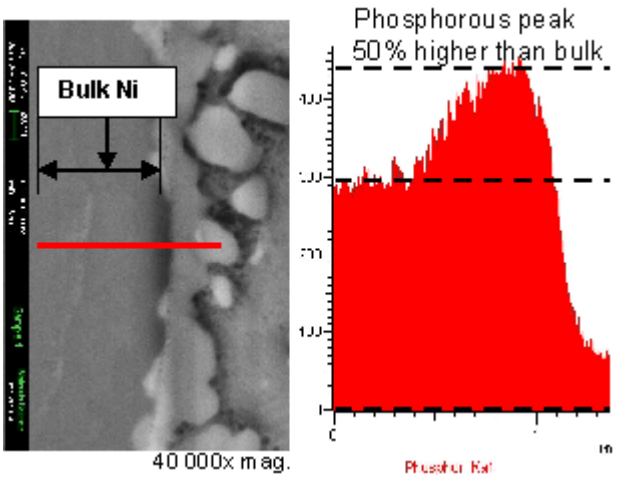

Fig. 26 SEM image of a cross-section of the Cu-Ni-Sn IMC on an 8.0% P nickel layer (Magnification 40,000x)

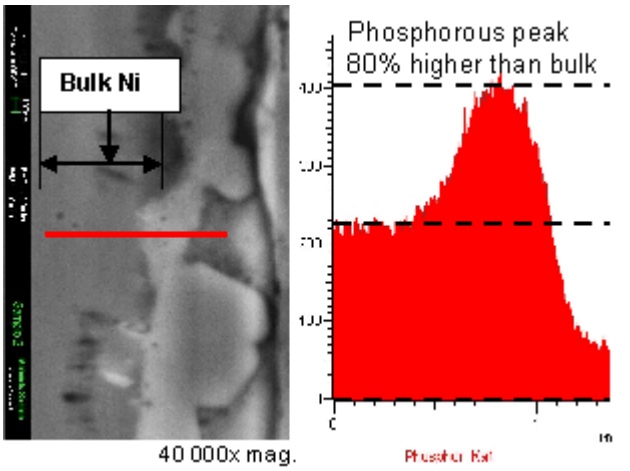

Fig 27: SEM image of a cross-section of the Cu-Ni-Sn IMC on an 11.2% P nickel layer (Magnification 40,000x)

The following table shows a significant difference in the P-content between the bulk nickel and interface between the solder and electroless nickel. Further analysis is still being conducted on samples that underwent thermo-cycling.

	8.0% P	**11.2% P**
Before soldering	8.1	11.2
After soldering	14.4	16.6
% Increase	78%	49%

As shown, the P-content enrichment is approximately 30% greater for the 8% P electroless nickel samples.

Basically there are two ways that phosphorus enrichment may occur:

1. Due to the immersion gold displacement reaction, nickel is removed and gold is deposited. Phosphorus is thus enriched at the interface

between the electroless nickel layer and the gold layer.

Assuming that a corrosion-resistant electroless nickel layer is less attacked by the immersion gold reaction (at the same gold solution parameters), the gold thickness will be lower compared to a less corrosion-resistant nickel layer. This was observed on 8.0% P nickel (gold thickness of 0.08µm) and on 11.2% nickel (gold thickness of 0.05µm). However, the tool used to measure the gold thickness is also limited in accuracy (typically +/- 0.01µm or greater) depending on pad size and collimator being used.

Previously collected data has shown that under normal operating conditions (immersion gold in the range 0.05-0.08µm), the phosphorus enrichment is less than one percent. Unless massive corrosion of grain boundaries occurs, the enrichment can be four percent or greater. As a general rule, it is expected that the more corrosion-resistant nickel will have lower phosphorus enrichment.

2. The second phosphorus enrichment occurs at the interface of nickel to solder during soldering, when the molten solder dissolves nickel and forms the Cu-Ni-Sn IMC. Again phosphorus enrichment occurs at the surface of the electroless nickel layer. The same corrosion resistance (as in the immersion gold reaction) is the driving force for more or less dissolution of nickel and causing phosphorus enrichment at the interface with solder.

In this case, the 11.2% P has lower phosphorus enrichment after soldering. Fundamentally, one could argue that this condition is due to the higher corrosion resistance, which affects not only the chemical behavior but also the physical properties, evidenced by the type of flat surface the high-P nickel produces. This flat structure, which occurs as a result of reduced surface area of nickel to solder, may also contribute to a lower dissolution of solder into the nickel. Furthermore, data to date shows that there is an impact on the type of IMC structure and composition that is produced and it is magnified by thermo-cycling of the product.

Returning to the difference in ball shear behavior by comparing the force length/diagrams, shown in Figures 11 12, the different behavior appears to be based on the difference of the formed IMC. Higher bulk phosphorus content in the electroless nickel does not necessarily mean a higher P-enrichment at the nickel to Cu-Ni-Sn interface. In case of the 11.2% P nickel layer, the amount of phosphorus enrichment at the interface had no impact on solder joint reliability. However, the 8.0% P nickel layer did show much higher variation in force.

Aluminum wire bond pull strength

Each wire bond pull test consisted of 50 pulls of a 32-µm AlSi-1 aluminum wire from Hereaus Figure 28 shows a series of aluminum wire pull strength forces from samples plated with different bulk P Nickel layers.

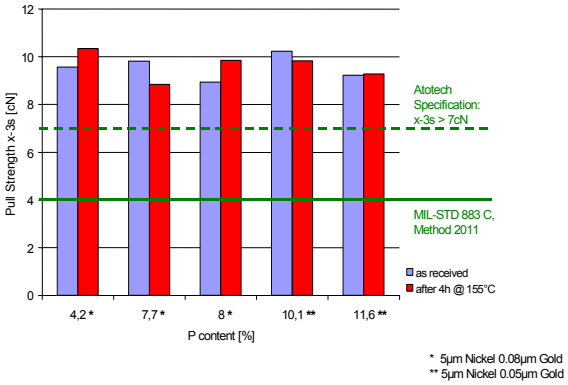

Fig. 28 Comparison of different bulk nickel phosphorus contents to aluminum-wire pull strength.

Samples “as received” or after annealing the layers for four hours at 155°C (prior to bonding) showed typical pull strength values of 9.5cN (+/- 0.75cN) for x-3s. These values are valid, regardless of the bulk nickel P-content, and far exceed MIL-STD 883 C, method 2011 (4cN).

Gold wire bond pull strength

Each wire bond pull test consisted of 60 pulls of a 30-µm Gold-Beta wire from Hereaus. Figure 32 shows a series of gold wire pull strength forces from samples plated with electrolytic nickel/gold or high-P ENIG. The electrolytic nickel/gold sample was intended as a reference and was used “as received” and after plasma-cleaning of the surface, whereas the ENIG sample with 11.2% P was used in “as received” condition.

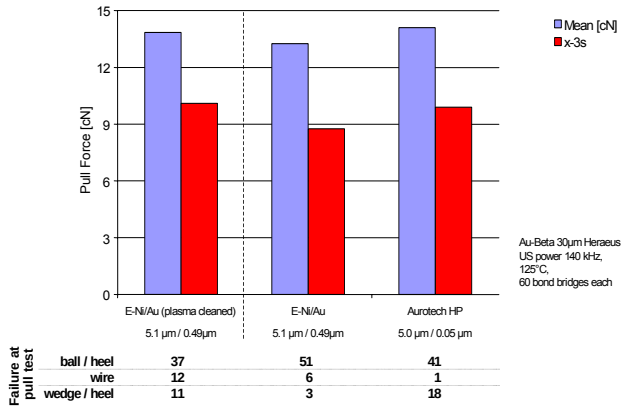

Fig. 29 Comparison of two different nickel/gold systems to gold-wire pull strength

As pull strength values for the plasma-cleaned electrolytic nickel/gold surface averaged 13.9cN, the non-plasma cleaned, high-P ENIG layer exceeded this value with 14.1cN. The average pull strength for

the non-plasma-cleaned electrolytic nickel/gold surface was the lowest, with 13.3cN.

Values for "x-3s", (covering 99.73% of all expected pull strength values) was achieved by plasma-cleaned electrolytic nickel/gold surface at 10.01cN, followed by the non-plasma-cleaned high-P ENIG layer with 9.9cN, and 8.8cN for the non-plasma-cleaned electrolytic nickel/gold surface.

CONCLUSIONS

1. The wettability/solderability of a gold thickness of average 0.05µm on high-P ENIG is equivalent to that of 0.08µm gold on a medium-P ENIG system. This might be based on the use of a denser, less porous gold layer, covering the high-P electroless nickel layer, and the fact that high-P nickel layers are more corrosion resistant and therefore less prone to show oxide layers on the surface.

2. A variation in electroless nickel and immersion gold thickness indicated an influence on the brittle fracture behavior. Lower nickel and higher gold thicknesses had the highest impact. However, in the case of higher phosphorus content (9.5 – 13 %) even at the lower nickel thickness there were no signs of brittle fracture. In addition, it can be observed that NSMD pads show better solder joint integrity, due to the enhanced area for anchorage.

3. After solder ball attachment and thermo-cycling (which induces stress to the solder joint), a clear benefit for a high-P electroless nickel layer is seen. The stress induced after 1000 thermo cycles did not influence the strength of the solder joint for the high-P electroless nickel layer. All force/length curves recorded were very consistent. In the case for medium-P electroless nickel, the layer showed a wide spread of all force/length curves, and comparing to "as received" samples, 7-9% P layers were negatively influenced by 1000 thermo cycles.

4. Upon investigation of the fractures (via cross-section after thermo-cycling) it was observed that the fracture for the medium-P system was occurring closer to the IMC, whereas in the case of the high-P this was further into the bulk solder. Additionally, it was observed that two types of IMC were created with structurally and chemically different compositions. A needle-like IMC structure is $(Ni,Cu)_3Sn_4$ with Ag_3Sn co-dispersed into the bulk solder. The chunky-like IMC structure is $(Cu,Ni)_6Sn_5$

5. The SEM images for the quantitative phosphorus distribution, showed approximately 30% less phosphorus enrichment (after the immersion gold reaction and soldering) at the interface of electroless nickel and Cu-Ni-Sn IMC using a high-P ENIG system. This finding agrees with previous studies in that the total amount of phosphorous at the interface is not the critical factor, rather the difference between the phosphorus content of the bulk electroless nickel layer and the P-enriched zone (between nickel and IMC) is the critical factor.

6. For aluminum-wire bonding there is no impact seen by varying the bulk nickel P-content, neither for "as received" samples nor for samples that have undergone annealing for four hours at 150°C. The capability for gold-wire bonding showed very good results for high-P electroless nickel with only one-tenth of the gold thickness used for electrolytic nickel/gold processes. This finding will be further investigated.

7. Based on this investigation, an ENIG system with a bulk nickel phosphorus concentration of 9.5- 13% shows advantages compared to a medium-P (7-9%) ENIG system. Both the solder joint reliability of the high-P system and the capability of the High P ENIG system allowing gold wire bondability are superior.

Based on this investigation, measurable advantages can be achieved using the recommended high-P ENIG system.
An electroless nickel layer, plated to a thickness of 5.5µm (+/- 0.5µm) with a phosphorus content of 9.5-13%, followed by an immersion gold layer of 0.05µm (+/- 0.02µm) will provide superior results regarding solder joint integrity and aluminum- and gold- wire bonding.

References:

1. Selective Finishing – Atotech Germany, "Impact of ENIG thickness to solder joint integrity on BGA pads", March 2003 Atotech

2. P. Backus, S. Lamprecht, High Phosphorus ENIG – highest resistance against corrosive environment, Proceedings of TPCA conference, 2002, October

3. Selective Finishing – Atotech Berlin / Rock Hill, "Black Pad versus Brittle Fracture", October 2002 Atotech

4. Selective Finishing – Atotech Germany, "Method of measuring the phosphorous content", February 2002 Atotech

5. Selective Finishing – Atotech Germany, "Aurotech – The most reliable Nickel/Gold process", January 2002 Atotech
6. S Lamprecht, "Aurotech SIT – The advanced Ni/Au-process for second image technology", Proceedings of IPC EXPO, September 2001

7. K. Johal, Study of the mechanism responsible for "Black pad" defect on PWB's using electroless nickel / immersion gold as final finish. Proceedings of IPC EXPO conference, 2001, April

8. F Cordes, R Huemoller, Electroless Nickel-Gold Is There a Future, Future circuits International.

9. Johal K, Are you in control of your electroless nickel/ Immersion gold process: Proceedings of IPC Works conference, 2000, September 14-19

10. F. D. Bruce Houghton, K Johal, D Cullen, E Huenger, M Toben, A Study on Interfacial Fracture Phenomena of Solder Joints Formed using the Electroless Nickel / Immersion Gold Surface Finish. Proceedings of IPC Works conference, 2000, September 9-19.

11. Johal Kuldip, Schreier H-J, Investigations on brittle fractures of BGA assemblies on ENIG surface finish, May 1999 Atotech

12. F. D. Bruce Houghton, ITRI Project on Electroless Nickel /Immersion Gold joint Cracking. Proceedings of IPC EXPO conference, 1999, March 14-18.

13. Biunno Nicholas, A root cause failure mechanism for solder joint integrity of electroless nickel/immersion gold surface finishes. Proceedings of IPC EXPO conference, 1999, March 14-18.

14. Mei Z, : The effect of electroless Ni/immersion Au plating parameters on PBGA solder joint attachment reliability: Proceedings of IPC conference, 1998, September 24-25

15. Bradley and K Banerji. Effects of PCB Finish on the Reliability and Wetting of Ball Grid Array Packages. May 1996

16. Riedel Wolfgang, Electroless Nickel Plating, ASM international

17. Young-Doo Jeon, Sabine Nieland, Andreas Ostmann, Herbert Reichl and Kyung-Wook Paik. A study on interfacial reaction between electroless Ni-P under bump metallization and Sn, Ag, Cu alloy. Journal of electronic materials 32, (6)